Proceedings of the ASME 2021
International Design Engineering Technical Conferences and
Computers and Information in Engineering Conference
IDETC-CIE2021
August 17-19, 2021, Virtual, Online

DETC2021-70011

TOWARDS TRANSPARENT MOTION PLANNING OF WEARABLE REHABILITATION EXOSKELETONS VIA MODEL-BASED ESTIMATION

Jiamin Wang, David Blankenship, Oumar Barry*
Department of Mechanical Engineering
Virginia Polytechnic Institute and State University
Blacksburg, Virginia 24061

ABSTRACT

We propose a novel online model-based motion planning algorithm for a family of rehabilitation exoskeletons to improve transparency in user-guided operation. In this study, we assume that the short-term human movement intention can be embedded in the time-delay dimensions of motion signals. The model-based estimation is employed to obtain the interaction load between the dynamical subsystems respectively controlled by the human and exoskeleton. The objective of the proposed motion planning algorithm is to reduce the interaction load, which leads to the establishment of a least-square optimization problem. A Support Vector Regression (SVR) model, driven by the time-delayed motion data, is implemented to solve the optimization problem by generating the acceleration of tracking reference. The motion planning algorithm based on SVR can be combined with a variety of trajectory tracking controllers. To ensure the efficiency of the algorithm for online applications, we also design the SVR model so that its properties can be calculated recursively based on latest data sets. The performance and characteristics of the motion planning algorithm are then observed and discussed through the control simulations of a wearable wrist exoskeleton designed for pathological tremor alleviation. The results show that while the planned tracking reference can approximate the synthetic human movement intention, the motion planning accuracy can be limited by system disturbances, and the delay of signals caused by digital filters.

*Corresponding Author (Email: obarry@vt.edu)

NOMENCLATURE

The mathematical notations used are listed as following:

- $\mathbf{F}(\underline{\mathbf{Z}})$ Single-input function $\mathbf{F}$ with argument $\mathbf{Z}$ (to differentiate from multiplications of parenthesized terms)
- $\|\mathbf{Z}\|_n$ n-norm of a matrix $\mathbf{Z}$ ($n = 2$ if not specified)
- $\mathbf{c}_m$ $m \times 1$ vector whose elements equal to $\mathbf{c} \in \mathbb{R}$
- $\mathbf{c}_{m\times n}$ $m \times n$ matrix whose elements equal to $\mathbf{c} \in \mathbb{R}$ (m, n fit with neighboring blocks if not specified)
- $\mathbf{I}_n$ Identity matrix of dimension n (m, n fit with neighboring blocks if not specified)
- $\mathbf{Z}^{-\mathrm{T}}$ Transposed inverse of $\mathbf{Z}$ (since $(\mathbf{Z}^{-1})^{\mathrm{T}} = (\mathbf{Z}^{\mathrm{T}})^{-1}$)
- $\mathbf{Z} > 0$ A square matrix $\mathbf{Z}$ is positive definite
- $\mathbf{Z}^{+}$ The Moore-Penrose pseudo inverse of $\mathbf{Z}$
- $\mathrm{diag}(\underline{\mathbf{z}})$ Convert a vector $\mathbf{z}$ into a diagonal matrix, whose diagonal elements are the elements of $\mathbf{z}$
- $\mathrm{vec}(\underline{\mathbf{Z}})$ Reshape a diagonal matrix $\mathbf{Z}$ into a column vector, whose elements are the diagonal elements of $\mathbf{Z}$

INTRODUCTION

The past decades have witnessed the emergence of many rehabilitation exoskeletons for physiotherapy and movement assistance [1,2]. To improve the safety and efficiency of exoskeleton operation, the control system of exoskeleton has been investigated extensively in previous studies [3–6]. The transparency in human-robot interaction, i.e., the minimization of resistance/reaction forces the robot applies to the user that leads to high compliance towards natural human motions [7], is crucial to the smoothness of user-guided control in rehabilitation exoskeletons [8]. While transparency can be evaluated by the interaction loading between

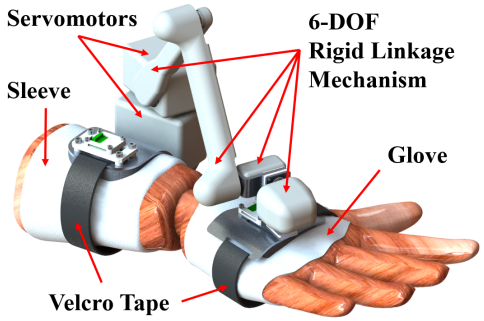

FIGURE 1: THE CAD DESIGN OF THE TREMOR ALLEVIATING WRIST EXOSKELETON (TAWE) [13].

the user and the exoskeleton [6, 7], it is challenging to obtain an ideal transparent exoskeleton that not only avoids encumbering the user, but also augments the movements following the exact intentions of the user. Some earlier studies effectively improved the exoskeleton transparency through model-based feedforward compensations and disturbance observer-based controllers [7, 9]. Other studies adopted user motion predictions for more compliant exoskeleton control or motion planning [6, 10–12]. In particular, the human intention of motion in these studies were predicted based on the user-applied loads, which were measured by force/torque sensors [6,10,12] or estimated through EMG signals and musculoskeletal models [11].

Our team is developing TAWE - a wearable wrist exoskeleton for pathological tremor alleviation as presented in Fig. 1 [13]. Unlike many stationary exoskeletons in the abovementioned studies, TAWE is not equipped with force sensors, and has limited computation and actuation capacities. The mechanism of TAWE is also back-drivable, which results in the dynamical interaction between user motions and exoskeleton controls. Finally, in the applications to pathological tremor suppression, the voluntary movements of the user can be overlaid by tremors, making it more difficult to identify the volitional intention of motions. These challenges were rarely addressed in previous studies. Therefore, the development of TAWE motivates us to explore efficient motion planning methods, which can be applied in real-time under system disturbances and tremors.

In the paper, we introduce a novel real-time motion planning algorithm for a family of rehabilitation exoskeletons to improve transparency in user-guided operation. The algorithm is proposed based on the assumption that the human movement intention in the short-term can be embedded in the time-delay dimensions of motion signals [14]. Model-based estimation is then employed to obtain the interaction load between the dynamical subsystems respectively controlled by the human and exoskeleton. The objective of the proposed motion planning algorithm is to reduce the interaction load, which leads to the establishment of a least-square optimization problem. A Support Vector Regression (SVR) model driven by the time-delayed motion data is implemented to solve the optimization problem by generating the acceleration of tracking reference. The motion planning algorithm based on SVR can be combined with a variety of trajectory tracking controllers. We also design the SVR model so that its properties can be calculated recursively based on a moving window of data sets, making it efficient for online applications.

The rest of the paper is arranged as follows: We first analyze the dynamical interplay in the human-exoskeleton control system, and proposed a few model assumptions. The optimization problem of motion planning is then proposed, which leads to the design of the SVR algorithm that calculates the exoskeleton tracking reference. Later, the performance and characteristics of the proposed motion planning algorithm is observed and discussed through the control simulations of TAWE. Finally, we summarize the findings of this paper and propose future works.

HUMAN-EXOSKELETON CONTROL SYSTEM

In this paper, we study the motion planning of a family of rehabilitation exoskeletons that follow a generic human-exoskeleton multibody model structure in the form of [5, 13]

$$\mathbf{M}(\mathbf{q})\ddot{\mathbf{q}} = -\mathbf{C}(\mathbf{q},\dot{\mathbf{q}})\dot{\mathbf{q}} - \mathbf{h}(t,\mathbf{q},\dot{\mathbf{q}}) + \mathbf{J}_w^{\mathrm{T}}(\mathbf{q})\mathbf{w} + \mathbf{u} \tag{1}$$

where $t \in \mathbb{R}_+$ is the time variable; $\mathbf{q} \in \mathbb{R}^{n_q}$ is the generalized coordinate; $\mathbf{w} \in \mathbb{R}^{n_w}$ is the bounded perturbation/disturbance; $\mathbf{M} \in \mathbb{R}^{n_q \times n_q}$ is the inertia matrix, which satisfies $\mathbf{M} = \mathbf{M}^{\mathrm{T}} > 0$; $\mathbf{C} \in \mathbb{R}^{n_q \times n_q}$ is the Coriolis and centripetal matrix; $\mathbf{h} \in \mathbb{R}^{n_q}$ is the vector of generalized forces, which includes potential energy forces and energy dissipation forces, and time-dependent excitations; and $\mathbf{J}_w \in \mathbb{R}^{n_w \times n_q}$ is the disturbance input Jacobian matrix.

For convenience, we define the control input as $\mathbf{u} = \mathbf{u}_1 + \mathbf{u}_2$, where $\mathbf{u}_1 \in \mathbb{R}^{n_q}$ and $\mathbf{u}_2 \in \mathbb{R}^{n_q}$ as the generalized control inputs from human and exoskeleton, respectively. These definitions are based on following assumptions:

(Asm. 1) The exoskeleton input $\mathbf{u}_e \in \mathbb{R}^{n_{u,e}}$ can actuate all the human degrees of freedom (DOF) within the closed kinematic chain, i.e, the human-exoskeleton system is fully-actuated. This leads to $n_{u,e} \geq n_q$, and

$$\mathbf{u}_2 = \mathbf{J}_{u,e}^{\mathrm{T}}\mathbf{u}_e \tag{2}$$

where $\mathbf{J}_{u,e} \in \mathbb{R}^{n_{u,e} \times n_q}$ is the exoskeleton input Jacobian matrix that satisfies $\mathrm{rank}(\mathbf{J}_{u,e}) = n_q$.

(Asm. 2) Uncertain loads from the user are generalized into direct forces/torques acting at the human joints, which are included in $\mathbf{h}$. Hence, we do not consider user load uncertainties as a part of $\mathbf{u}_1$. We also assume that the uncertainties include pathological tremor effects.

With a smooth tracking reference $\mathbf{r}(t) \in \mathbb{R}^{n_q}$, the tracking error and control system state can be defined as

$$\boldsymbol{\varepsilon} = \mathbf{q} - \mathbf{r}; \quad \mathbf{x} = \left[\boldsymbol{\varepsilon}^{\mathrm{T}} \ \dot{\boldsymbol{\varepsilon}}^{\mathrm{T}}\right]^{\mathrm{T}} \tag{3}$$

Then we can write the control system of Eq.(1) as

$$\dot{\mathbf{x}} = \begin{bmatrix} \dot{\boldsymbol{\varepsilon}} \\ -\ddot{\mathbf{r}} - \mathbf{M}^{-1}(\mathbf{C}\dot{\mathbf{q}} + \mathbf{h} - \mathbf{J}_w^{\mathrm{T}}\mathbf{w}) \end{bmatrix} + \begin{bmatrix} \mathbf{0} \\ \mathbf{M}^{-1} \end{bmatrix} \mathbf{u} \tag{4}$$

For human-exoskeleton cooperative control, it is important to note that the human control input $\mathbf{u}_1$ follows a tracking reference (i.e., the true human intention of movement) different from that followed by the exoskeleton input $\mathbf{u}_2$. To avoid confusion, we assume the user movement intention as an unknown tracking reference $\mathbf{r}_1(t) \in \mathbb{R}^{n_q}$, and the known tracking reference followed by the exoskeleton is defined as $\mathbf{r}_2(t) \in \mathbb{R}^{n_q}$.

Assumptions on Human Control Input Dynamics

When $\mathbf{u}_2 \approx \mathbf{0}$, i.e., the exoskeleton serves as only a passive load, the user input $\mathbf{u}_1$ controls the human-exoskeleton system to follow $\mathbf{r} = \mathbf{r}_1$. However, due to the complexity of human neuro-musculoskeletal system [15], the unknown dynamics of $\mathbf{u}_1$ can be volatile and extremely complicated. Hence, we propose two more assumptions to simplify the analysis:

(Asm. 3) Within a delayed time window $t \in \mathbb{T}$, the short-term dynamics of $\mathbf{u}_1$ can be approximated by a nonlinear function α as [14]

$$\mathbf{u}_1 \approx \alpha(\mathbf{z}_q, \mathbf{z}_{r,1}) \tag{5}$$

with

$$\mathbf{z}_q = \begin{bmatrix} \mathbf{q}_{t,1}^{\mathrm{T}} & \mathbf{q}_{t,2}^{\mathrm{T}} & \cdots & \mathbf{q}_{t,m}^{\mathrm{T}} \end{bmatrix}^{\mathrm{T}};\ \mathbf{z}_{r,i} = \begin{bmatrix} \mathbf{r}_{i,t,1}^{\mathrm{T}} & \mathbf{r}_{i,t,2}^{\mathrm{T}} & \cdots & \mathbf{r}_{i,t,m}^{\mathrm{T}} \end{bmatrix}^{\mathrm{T}} \tag{6}$$

where $\mathbf{q}_{t,i},\ \mathbf{r}_{t,i} \in \mathbb{R}^{n_q}$ (where $i = 1,\ 2, \cdots,\ m$) are the generalized coordinate and tracking reference at time $t_i \in \mathbb{T}$, respectively.

(Asm. 4) The control input α can adapt to property changes in the human-exoskeleton dynamical system, and eliminate steady-state tracking errors.

Hence, (Asm. 3) embeds the user input in the time-delay dimensions of human intentions and movements [14], and takes into consideration the time-delay effects in the system. Although the true nature of α is unknown, a variety of controllers can fulfill the requirements of (Asm. 4) under certain conditions. As an example, when the dynamical properties of the model is time-invariant, and the user motion is very slow, we obtain $\dot{\mathbf{M}} \approx \mathbf{0}$. Then we can design a Proportional-Integral-Derivative (PID) controller

$$\mathbf{u}_1 = \mathbf{u}_{1,\mathrm{PID}} = -(c_{u,1,\mathrm{I}}\boldsymbol{\varepsilon}_{\mathrm{I}} + c_{u,1,\mathrm{P}}\boldsymbol{\varepsilon} + c_{u,1,\mathrm{D}}\dot{\boldsymbol{\varepsilon}}) \tag{7}$$

where

$$\boldsymbol{\varepsilon}_{\mathrm{I}} = \int_0^t (\mathbf{q}(\tau) - \mathbf{r}(\tau))d\tau \tag{8}$$

is the integral of tracking error; and $c_{u,1,\mathrm{I}},\ c_{u,1,\mathrm{P}},\ c_{u,1,\mathrm{D}} > 0$ are respectively the P, I, and D gains. A stabilizing PID controller from Eq.(7) requires a Hurwitz state matrix [13]

$$\mathbf{A} = \begin{bmatrix} \mathbf{0} & \mathbf{I} & \mathbf{0} \\ \mathbf{0} & \mathbf{0} & \mathbf{I} \\ -c_{u,1,\mathrm{I}}\mathbf{M}^{-1} & -c_{u,1,\mathrm{P}}\mathbf{M}^{-1} & -c_{u,1,\mathrm{D}}\mathbf{M}^{-1} \end{bmatrix} \tag{9}$$

Since $\mathbf{M} > 0$, the eigenvalues κ_A of $\mathbf{A}$ can be solved from a set of n_q characteristic equations

$$\kappa_{M,i}\kappa_A^3 + c_{u,1,\mathrm{D}}\kappa_A^2 + c_{u,1,\mathrm{P}}\kappa_A + c_{u,1,\mathrm{I}} = 0\ (i = 1,\ 2,\ \cdots,\ n_q) \tag{10}$$

where $\kappa_{M,i}$ is the ith eigenvalue of $\mathbf{M}$. The Routh-Hurwitz criterion for $\mathbf{A}$ requires that the control parameters satisfy $c_{u,1,\mathrm{P}}c_{u,1,\mathrm{D}} > c_{u,1,\mathrm{I}}\kappa_{M,i}$ for every characteristic equation. Again, while a PID controller can eliminate steady-state errors, the controller from Eq.(7) has very restrictive application conditions, which will be applied only in the simulations in later sections.

Adaptive Controller for Exoskeleton

When $\mathbf{u}_1 \approx \mathbf{0}$, i.e., the user is not actively controlling the movements, the human-exoskeleton system can be controlled to track an arbitrarily designed know trajectory $\mathbf{r} = \mathbf{r}_2$ via $\mathbf{u}_2$. Here, we define $\mathbf{p} \in \mathbb{R}^{n_p}$ as the uncertain dynamical parameters of the model based on the following assumption:

(Asm. 5) The dynamical properties of the model (i.e., $\mathbf{M}$, $\mathbf{C}$, and $\mathbf{h}$) are bounded and time-invariant (or slowly time-varying). This leads to $\dot{\mathbf{p}} \approx \mathbf{0}$.

Hence, an adaptive controller $\mathbf{u}_2$ and its parameter estimation update law can be designed as [5]

$$\mathbf{u}_2 = \mathbf{J}_p^{\mathrm{T}}(t, \mathbf{q}, \dot{\mathbf{q}})\hat{\mathbf{p}} + \mathbf{u}_f + \mathbf{u}_b; \tag{11a}$$

$$\dot{\hat{\mathbf{p}}} = -\Gamma^{-1}\mathbf{J}_p\xi \tag{11b}$$

with the intermediate terms $\mathbf{u}_f,\ \mathbf{u}_b,\ \zeta,\ \xi \in \mathbb{R}^{n_q}$ defined as

$$\mathbf{u}_f = \mathbf{M}_0\dot{\zeta} + \mathbf{C}_0\zeta + \mathbf{h}_0; \quad \mathbf{u}_b = -\mathbf{R}(\mathbf{q})\xi \tag{12a}$$

$$\zeta = \dot{\mathbf{r}} - \mathbf{K}_1\boldsymbol{\varepsilon}; \quad \xi = \dot{\boldsymbol{\varepsilon}} + \mathbf{K}_1\boldsymbol{\varepsilon} \tag{12b}$$

where $\Gamma,\ \mathbf{R},\ \mathbf{K}_1 \in \mathbb{R}^{n_q \times n_q}$ are symmetric positive definite matrices; $\mathbf{M}_0$, $\mathbf{C}_0$, and $\mathbf{h}_0$ are the known dynamical properties and follows the definitions of $\mathbf{M}$, $\mathbf{C}$, and $\mathbf{h}$, respectively; $\hat{\mathbf{p}}$ is the estimation of $\mathbf{p}$; and $\mathbf{J}_p$ is the Jacobian matrix of $\mathbf{p}$ which satisfies [5]

$$\mathbf{J}_p^{\mathrm{T}}\mathbf{p} + \mathbf{u}_f = \mathbf{M}\dot{\zeta} + \mathbf{C}\zeta + \mathbf{h} \tag{13}$$

When disturbance $\mathbf{w} \approx \mathbf{0}$, the adaptive controller can stabilize Eq.(4) by converging the Lyapunov function designed as

$$\mathscr{V} = (\xi^{\mathrm{T}}\mathbf{M}\xi + \boldsymbol{\varepsilon}^{\mathrm{T}}\mathbf{K}_2\boldsymbol{\varepsilon} + \tilde{\mathbf{p}}^{\mathrm{T}}\Gamma\tilde{\mathbf{p}})/2 \tag{14}$$

where $\tilde{\mathbf{p}} = \hat{\mathbf{p}} - \mathbf{p}$, and $\mathbf{K}_2 \in \mathbb{R}^{n_q \times n_q}$ satisfies $\mathbf{K}_2 = \mathbf{K}_2^{\mathrm{T}} > 0$. The stability proof of Eq.(14) can be referenced from [5]. Compared to the PID controller in Eq.(7), the adaptive controller in Eq.(11) is more rigorous and suitable for exoskeletons.

It should be noted that the adaptive controller from Eq.(11) can also be used to identify the uncertain dynamical parameters (e.g., mass and moments) of the human-exoskeleton model. This,

again, requires that the user does not actively control the movements. When there are no model uncertainties ($\mathbf{p} = 0$), the above controller is reduced to a Proportional-Derivative (PD) trajectory tracking controller for multibody system.

Interaction between Human and Exoskeleton

This subsection discusses the dynamical interplay between the human and exoskeleton, which considers the existences of both $\mathbf{u}_1$ and $\mathbf{u}_2$. This requires a final model assumption on the pathological tremors, disturbances, and sensor noises:

(Asm. 6) The pathological tremors, disturbances, and sensor noises mostly belong to bands of noticeably higher frequencies than those of voluntary user motions and exoskeleton tracking references.

Hence, we modify Eq.(1) into a dynamical model in the low-frequency domain

$$\bar{\mathbf{M}}(\underline{\bar{\mathbf{q}}})\ddot{\bar{\mathbf{q}}} = -\bar{\mathbf{C}}(\bar{\mathbf{q}},\dot{\bar{\mathbf{q}}})\dot{\bar{\mathbf{q}}} - \bar{\mathbf{h}}(t,\bar{\mathbf{q}},\dot{\bar{\mathbf{q}}}) + \mathbf{v} + \bar{\alpha} + \bar{\mathbf{u}}_2 \tag{15}$$

where "$\bar{}$" denotes low-pass filtered properties, and $\mathbf{v} \in \mathbb{R}^{n_q}$ contains unfiltered model disturbances and the perturbation caused by low-pass filtering, which is assumed to be bounded. Specifically, $\bar{\mathbf{h}}$ and $\bar{\mathbf{u}}_2$ does not contain terms related to tremors. Also, based on (Asm. 3) and (Asm. 5), we obtain $\bar{\alpha} = \alpha(\bar{\mathbf{z}}_q, \mathbf{z}_{r,1})$, where $\mathbf{z}_{r,1}$ is not affected by low-pass filtering.

By considering that the user and exoskeleton each controls a part of the human-robot control system, we separate Eq.(15) into two dynamical subsystems

$$\bar{\mathbf{M}}_1\ddot{\bar{\mathbf{q}}} = -\bar{\mathbf{C}}_1\dot{\bar{\mathbf{q}}} - \bar{\mathbf{h}}_1 + \bar{\alpha} - \lambda \tag{16a}$$

$$\bar{\mathbf{M}}_2\ddot{\bar{\mathbf{q}}} = -\bar{\mathbf{C}}_2\dot{\bar{\mathbf{q}}} - \bar{\mathbf{h}}_2 + \bar{\mathbf{u}}_2 + \mathbf{v} + \lambda \tag{16b}$$

where $\bar{\mathbf{M}}_i$, $\bar{\mathbf{C}}_i$, and $\bar{\mathbf{h}}_i$ (with $i = 1,\ 2$) are the components of $\bar{\mathbf{M}}$, $\bar{\mathbf{C}}$, and $\bar{\mathbf{h}}$, respectively. In particular, $\bar{\mathbf{M}}_i$ satisfies $\bar{\mathbf{M}}_i = \bar{\mathbf{M}}_i^{\mathrm{T}} > 0$. We introduce λ as the generalized interaction force between the two subsystems.

In a few studies [6, 12], λ is obtained through fused measurements from multiple sensors, which indicate the intention of movements, where Eq.(16a) and Eq.(16b) have fixed structures as the human and exoskeleton subsystems, respectively. In this study, we consider that the exoskeleton only provides partial movement assistance, which is reasonable for wearable devices due to their power capacity limitations. Hence, the dynamical properties of Eq.(16b) can be designed arbitrarily based on the level of movement assistance. The adaptive controller in Eq.(11) can be used to obtain the estimated properties $\hat{\mathbf{M}}$, $\hat{\mathbf{C}}$, and $\hat{\mathbf{h}}$, so that the properties of Eq.(16b) are reasonably designed.

Finally, based on Eq.(16a), we can represent λ as

$$\lambda = \bar{\alpha} - \bar{\mathbf{M}}_1\ddot{\bar{\mathbf{q}}} - \bar{\mathbf{C}}_1\dot{\bar{\mathbf{q}}} - \bar{\mathbf{h}}_1 \tag{17}$$

which involves the voluntary intention of movements. On the other hand, similar to Eq.(11), we can design the controller $\mathbf{u}_2$ so

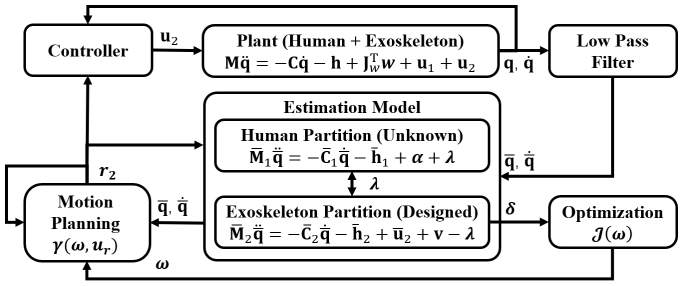

FIGURE 2: THE FRAMEWORK OF THE PROPOSED EXOSKELETON MOTION PLANNING ALGORITHM.

that its filter version can be written as

$$\bar{\mathbf{u}}_2 = \bar{\mathbf{M}}_2\dot{\zeta} + \bar{\mathbf{C}}_2\zeta + \bar{\mathbf{h}}_2 - \bar{\mathbf{R}}(\underline{\bar{\mathbf{q}}})\bar{\xi} \tag{18}$$

Hence, λ can be estimated from Eq.(16b) as

$$\lambda \approx \beta(\bar{\mathbf{z}}_q, \mathbf{z}_{r,2}) \approx \bar{\mathbf{M}}_2\ddot{\bar{\xi}} + \bar{\mathbf{C}}_2\bar{\xi} - \bar{\mathbf{R}}(\underline{\bar{\mathbf{q}}})\bar{\xi} \tag{19}$$

While Eq.(17) and Eq.(19) represents the identical λ, the human intention $\mathbf{r}_1$ is embedded implicitly in the nonlinear dynamics of $\bar{\mathbf{q}}$. The dynamics of $\mathbf{r}_1$ and α, again, are extremely difficult to model. However, λ estimated via Eq.(19) can reflect the coordination level between the human and robot. Small λ magnitudes indicate that the exoskeleton can cooperatively control the designated subsystem Eq.(16b) following the user intention. In the next section, we discuss the real-time motion planning of $\mathbf{r}_2$. The objective of motion planning is to minimize λ.

REAL-TIME MOTION PLANNING

This section discusses the motion planning of $\mathbf{r}_2$ that minimizes λ for the user-guided exoskeleton control. The general motion planning framework is shown in Fig. 2. The motion planning algorithm is established on the discrete-time domain with

$$t = k/c_s \tag{20}$$

where k is the discrete time used to label discrete-time variables; and $c_s > 0$ is the sampling frequency in Hz. By defining a window $\mathbb{T}_{k,m}$ at discrete time k with m delays, we propose the motion planning scheme of $\mathbf{r}_2$ as

$$\mathbf{r}_{2,k+1} = \mathbf{r}_{2,k} + \dot{\mathbf{r}}_{2,k}/c_s; \quad \dot{\mathbf{r}}_{2,k+1} = \dot{\mathbf{r}}_{2,k} + \ddot{\mathbf{r}}_{2,k}/c_s \tag{21}$$

with the approximation

$$\ddot{\mathbf{r}}_{2,k} \approx \gamma_k(\omega, \mathbf{u}_{r,k}); \quad \mathbf{u}_{r,k} = \left[\bar{\mathbf{z}}_{q,k,m}^{\mathrm{T}}\ \mathbf{z}_{r,2,k,m}^{\mathrm{T}}\right]^{\mathrm{T}} \tag{22}$$

where $\gamma \in \mathbb{R}^{n_q}$ is a nonlinear function; ω is the tunable model parameters; $\bar{\mathbf{z}}_{q,k}$ and $\mathbf{z}_{r,2,k}$ are collection vectors of time-delayed terms from $\mathbb{T}_{k,m}$ defined as

$$\bar{\mathbf{z}}_{q,k,m} = \left[\bar{\mathbf{q}}_k^{\mathrm{T}}\ \bar{\mathbf{q}}_{k-1}^{\mathrm{T}}\ \cdots\ \bar{\mathbf{q}}_{k-m}^{\mathrm{T}}\right]^{\mathrm{T}};\ \mathbf{z}_{r,2,k,m} = \left[\mathbf{r}_{2,k}^{\mathrm{T}}\ \mathbf{r}_{2,k-1}^{\mathrm{T}}\ \cdots\ \mathbf{r}_{2,k-m}^{\mathrm{T}}\right]^{\mathrm{T}} \tag{23}$$

Hence, based on Eq.(16b) and Eq.(18), we introduce δ as

$$\delta_k = \bar{\mathbf{M}}_{2,k}^{-1}(\lambda_k + \mathbf{v}_k) = \ddot{\bar{\mathbf{q}}}_k - \gamma_k + \mathbf{z}_{\delta,k} \tag{24}$$

where the intermediate term $\mathbf{z}_\delta$ is

$$\mathbf{z}_{\delta,k} = \mathbf{K}_1\bar{\varepsilon}_k + \bar{\mathbf{M}}_{2,k}^{-1}\bar{\mathbf{C}}\bar{\dot{\xi}}_k + \bar{\mathbf{M}}_{2,k}^{-1}\bar{\mathbf{R}}_k\bar{\xi}_k \tag{25}$$

and $\ddot{\bar{\mathbf{q}}}_k$ is numerically approximated by

$$\ddot{\bar{\mathbf{q}}}_k \approx c_s^2(\bar{\mathbf{q}}_{k+1} - 2\bar{\mathbf{q}}_k + \bar{\mathbf{q}}_{k-1}) \tag{26}$$

When $\mathbf{v}$ is small, δ is comparable to λ. As the objective of motion planning is to minimize λ, the basic least square cost function of the motion planning optimization is proposed as

$$\mathscr{J}(\underline{\hat{\omega}_k}) = (\hat{\omega}_k^{\mathrm{T}}\mathbf{P}\hat{\omega}_k + \mathbf{z}_{\delta,k,\mu}^{\mathrm{T}}\mathbf{Q}\mathbf{z}_{\delta,k,\mu})/2 \tag{27}$$

where $\mathbf{P}$ and $\mathbf{Q}$ are positive definite diagonal matrices, and $\mathbf{z}_{y,k,\mu}$ is a collection vector of δ over a window $\mathbb{T}_{k,\mu}$ at discrete time k with μ delays, which is defined as

$$\mathbf{z}_{\delta,k,\mu} = \begin{bmatrix}\delta_k^{\mathrm{T}} & \delta_{k-1}^{\mathrm{T}} & \cdots & \delta_{k-\mu}^{\mathrm{T}}\end{bmatrix}^{\mathrm{T}} \tag{28}$$

The optimization problem is solved by minimizing $\mathscr{J}$, which yields the estimated parameter $\hat{\omega}$ that minimizes δ over the window $\mathbb{T}_{k,\mu}$. The estimated parameter $\hat{\omega}$ at discrete time k is then used for the upcoming motion planning of $\mathbf{r}_2$. It should be noted that $\mathscr{J}$ can be modified to consider additional criteria including safety and range of motion constraints. There is also a variety of options for the structure of γ and the optimizer for $\mathscr{J}$. The next subsection discusses an approach to the motion planning of $\mathbf{r}_2$ using online Support Vector Regression.

Online Support Vector Regression

Support Vector Regression (SVR) is the application of Support Vector Machine (SVM) in regression [16–19], which is model-free and capable of handling nonlinearities. The least square SVR nonlinearly maps the input data into a higher-dimensional feature space, and performs linear regression on the nonlinear mappings of input data. Based on the least square cost function Eq.(27), we employ SVR for the identification of γ used in motion planning. Hence, the function of γ can be written as

$$\gamma_k = \Omega\phi_k(\underline{\mathbf{u}_{r,k}}) + \mathbf{b} + \mathbf{C}_p\bar{\dot{\xi}}_k; \quad \Omega = \begin{bmatrix}\omega_1 & \omega_2 & \cdots & \omega_{n_q}\end{bmatrix}^{\mathrm{T}} \tag{29}$$

where $\mathbf{b} \in \mathbb{R}^{n_q}$ is the bias; $\mathbf{C}_p = \mathbf{C}_p^{\mathrm{T}} > 0$ is a constant coefficient matrix; and $\phi \in \mathbb{R}^{n_q}$ is the nonlinear projection of input $\mathbf{u}_r$ from Eq.(22); ω_i (with $i = 1,\ 2,\ \cdots,\ n_q$) are derived from

$$\omega = \begin{bmatrix}\omega_1^{\mathrm{T}} & \omega_2^{\mathrm{T}} & \cdots & \omega_{n_q}^{\mathrm{T}}\end{bmatrix}^{\mathrm{T}} \tag{30}$$

The impedance term $\mathbf{C}_p\bar{\dot{\xi}}_k$ is introduced to improve the stability of $\mathbf{r}_2$, and prevent it from drifting far away from the current coordinate. Hence, based on Eq.(24) and Eq.(29), we introduce the output $\mathbf{y}$ as

$$\mathbf{y}_k = c_s^2(\bar{\mathbf{q}}_{k+1} - 2\bar{\mathbf{q}}_k + \bar{\mathbf{q}}_{k-1}) + \mathbf{z}_{\delta,k} - \mathbf{C}_p\bar{\dot{\xi}}_k \tag{31}$$

This representation also indicate that $\mathbf{C}_p$ should be reasonably selected, so that it does not significantly affect the robustness of adaptive controller.

Based on the above setups, the Lagrangian function of the optimization problem can be established as

$$\mathscr{L}(\underline{\hat{\omega}_k}) = \mathscr{J}(\underline{\hat{\omega}_k}) - \theta_k^{\mathrm{T}}\mathbf{z}_{r,y,\mu} \tag{32}$$

where θ is the Lagrange multiplier vector corresponding to a collection of constraints $\mathbf{z}_{r,y}$ defined as

$$\mathbf{z}_{r,y,\mu} = \begin{bmatrix}\mathbf{r}_{y,k}^{\mathrm{T}} & \mathbf{r}_{y,k-1}^{\mathrm{T}} & \cdots & \mathbf{r}_{y,k-\mu}^{\mathrm{T}}\end{bmatrix}^{\mathrm{T}} \tag{33a}$$

$$\mathbf{r}_{y,k-i} = \hat{\Omega}_k\phi_{k-i} + \delta_{k-i} + \hat{\mathbf{b}}_k - \mathbf{y}_{k-i} \quad (i = 0,\ 1,\ \cdots,\ \mu) \tag{33b}$$

In this study, we simplify the cost function so that $\mathbf{P} = \mathbf{I}$, and $\mathbf{Q} = (1/c_Q)\mathbf{I}$ where $c_Q > 0$. The Karush-Kuhun-Tucker (KKT) conditions is formulated for the dual problem of Eq.(32) as [16]

$$\frac{\partial\mathscr{L}}{\partial\hat{\omega}_k} = 0 \ \rightarrow \hat{\omega}_{i,k} = \Phi_k\theta_{B,i,k} \quad (i = 1,\ 2,\ \cdots,\ n_q) \tag{34a}$$

$$\frac{\partial\mathscr{L}}{\partial\mathbf{z}_{\delta,k,m}} = 0 \ \rightarrow \delta_{k-i} = c_Q\theta_{A,i,k} \quad (i = 0,\ 1,\ \cdots,\ \mu) \tag{34b}$$

$$\frac{\partial\mathscr{L}}{\partial\hat{\mathbf{b}}_k} = 0 \ \rightarrow \mathbf{1}_{1,\mu}\theta_{B,i,k} = \mathbf{0} \quad (i = 1,\ 2,\ \cdots,\ n_q) \tag{34c}$$

$$\frac{\partial\mathscr{L}}{\partial\theta} = 0 \ \rightarrow \mathbf{r}_{y,k-i} = \mathbf{0} \quad (i = 0,\ 1,\ \cdots,\ \mu) \tag{34d}$$

where the intermediate terms are derived from

$$\Phi_k = \begin{bmatrix}\phi_k & \phi_{k-1} & \cdots & \phi_{k-\mu}\end{bmatrix}; \quad \theta_k = \begin{bmatrix}\theta_{A,0,k}^{\mathrm{T}} & \theta_{A,1,k}^{\mathrm{T}} & \cdots & \theta_{A,\mu,k}^{\mathrm{T}}\end{bmatrix}^{\mathrm{T}} \tag{35a}$$

$$\Theta_k = \begin{bmatrix}\theta_{A,0,k} & \theta_{A,1,k} & \cdots & \theta_{A,\mu,k}\end{bmatrix}^{\mathrm{T}} = \begin{bmatrix}\theta_{B,1,k} & \theta_{B,2,k} & \cdots & \theta_{B,n_q,k}\end{bmatrix} \tag{35b}$$

Based on the substitutions of ω and θ, the KKT conditions yields the least square problem

$$\begin{bmatrix}\mathbf{Y}_k & \mathbf{0}_{n_q,1}\end{bmatrix}\Pi_k^{-1} = \begin{bmatrix}\hat{\Theta}_k^{\mathrm{T}} & \hat{\mathbf{b}}_k\end{bmatrix} \tag{36}$$

where

$$\Pi_k = \begin{bmatrix}\Phi_k^{\mathrm{T}}\Phi_k + c_Q\mathbf{I} & \mathbf{1}_{\mu,1} \\ \mathbf{1}_{1,\mu} & 0\end{bmatrix}; \quad \mathbf{Y}_k = \begin{bmatrix}\mathbf{y}_k & \mathbf{y}_{k-1} & \cdots & \mathbf{y}_{k-\mu}\end{bmatrix} \tag{37}$$

By employing the radial basis function (RBF) kernal function [19] designed as

$$\mathscr{K}(\mathbf{u}_{r,k-i}, \mathbf{u}_{r,k-j}) = \phi_i^{\mathrm{T}}\phi_j = \exp(-\|\mathbf{u}_{r,i} - \mathbf{u}_{r,j}\|^2/c_{\mathscr{K}}^2) \tag{38}$$

where $i,\ j = 0,\ 1,\ \cdots,\ \mu$ and $c_{\mathscr{K}} > 0$, γ at discrete time $k+1$ is calculated based on the model driven by previous data as

$$\gamma_{k+1} = \begin{bmatrix}\hat{\Theta}_k^{\mathrm{T}} & \hat{\mathbf{b}}_k\end{bmatrix}\begin{bmatrix}\Phi_k^{\mathrm{T}}\phi_{k+1} \\ 1\end{bmatrix} + \mathbf{C}_p\bar{\dot{\xi}}_{k+1} = \begin{bmatrix}\hat{\Theta}_k^{\mathrm{T}} & \hat{\mathbf{b}}_k\end{bmatrix}\begin{bmatrix}\psi_k \\ 1\end{bmatrix} + \mathbf{C}_p\bar{\dot{\xi}}_{k+1} \tag{39}$$

where ψ is a collection vector of kernel terms

$$\psi_k = \begin{bmatrix}\mathscr{K}(\hat{\mathbf{u}}_{r,k+1}, \mathbf{u}_{r,k}) \\ \mathscr{K}(\hat{\mathbf{u}}_{r,k+1}, \mathbf{u}_{r,k-1}) \\ \vdots \\ \mathscr{K}(\hat{\mathbf{u}}_{r,k+1}, \mathbf{u}_{r,k-m})\end{bmatrix}^{\mathrm{T}} \tag{40}$$

As previously mentioned, it is crucial to ensure the efficiency of the motion planning algorithm so that it can operate on line. To obtain θ in real-time [17], we employ an iterative approach to calculate the update of Π^{-1} based on data in a moving window. When the data of $\bar{\mathbf{q}}_{k+2}$ is available for the calculation of $\mathbf{y}_{k+1}$, we obtain an augmented matrix as

$$\Pi_{k,k+1} = \begin{bmatrix} 1+c_Q & \begin{bmatrix}\phi_{k+1}^{\mathrm{T}}\Phi_k & 1\end{bmatrix} \\ \begin{bmatrix}\Phi_k^{\mathrm{T}}\phi_{k+1} \\ 1\end{bmatrix} & \Pi_k \end{bmatrix} \tag{41}$$

By defining an intermediate vector

$$\mathbf{z}_{\mathscr{K},k,i} = \begin{bmatrix}\Phi_k^{\mathrm{T}}\phi_{k-i} \\ 1\end{bmatrix} \quad (i=-1,\ 0,\ 1,\ \cdots,\ \mu) \tag{42}$$

which can be calculated using the RBF kernel function, we can obtain based on Schur complement [20] that

$$\Pi_{k,k+1}^{-1} = \begin{bmatrix} z_{\Pi,2} & -z_{\Pi,2}\mathbf{z}_{\Pi,1}^{\mathrm{T}} \\ -z_{\Pi,2}\mathbf{z}_{\Pi,1} & \Pi_k^{-1} + z_{\Pi,2}\mathbf{z}_{\Pi,1}\mathbf{z}_{\Pi,1}^{\mathrm{T}} \end{bmatrix} \tag{43}$$

where

$$\mathbf{z}_{\Pi,1} = \Pi_k^{-1}\mathbf{z}_{\mathscr{K},k,-1}; \quad z_{\Pi,2} = 1/(1+c_Q - \mathbf{z}_{\mathscr{K},k,-1}^{\mathrm{T}}\mathbf{z}_{\Pi,1}) \tag{44}$$

After that, with $\Pi_{k,k+1}^{-1}$ alternatively presented via intermediate terms as

$$\Pi_{k,k+1}^{-1} = \begin{bmatrix}\mathbf{Z}_{\Pi,3} & \mathbf{Z}_{\Pi,4} \\ \mathbf{Z}_{\Pi,4}^{\mathrm{T}} & \mathbf{Z}_{\Pi,5}\end{bmatrix} \tag{45}$$

where $\mathbf{Z}_{\Pi,5}$ is a 2×2 matrix. We can then obtain

$$\mathbf{Z}_{\Pi,6} = \mathbf{Z}_{\Pi,3} - \mathbf{Z}_{\Pi,4}\mathbf{Z}_{\Pi,5}^{-1}\mathbf{Z}_{\Pi,4}^{\mathrm{T}} \tag{46}$$

Finally, the updated Π^{-1} can be calculated as

$$\Pi_{k+1}^{-1} = \begin{bmatrix} \mathbf{Z}_{\pi,6} + z_{\Pi,8}\mathbf{z}_{\Pi,7}\mathbf{z}_{\Pi,7}^{\mathrm{T}} & -z_{\Pi,8}\mathbf{z}_{\Pi,7} \\ -z_{\Pi,8}\mathbf{z}_{\Pi,7}^{\mathrm{T}} & z_{\Pi,8} \end{bmatrix} \tag{47}$$

where

$$\mathbf{z}_{\Pi,7} = \mathbf{Z}_{\Pi,6}\mathbf{1}_{\mu,1}; \quad z_{\Pi,8} = -1/(\mathbf{1}_{1,\mu}\mathbf{z}_{\Pi,7}) \tag{48}$$

Therefore, Π^{-1} can be efficiently updated online through the above process efficiently without matrix inversion computations.

Remarks on the Proposed Method

In summary, the proposed motion planning algorithm is designed based on the objective of minimizing interaction load λ between the user and exoskeleton, which leads to the parameters Θ and $\mathbf{b}$ used in the planning of tracking reference acceleration $\dot{\mathbf{r}}_2$ through Eq.(39). The algorithm can be combined with a variety of controllers, and does not require measurements of acceleration or force/torque. The employed online SVR algorithm provides an efficient data-driven method to realize nonlinear motion planning. It should be noted that the RBF kernel adopted in this study can also be replaced by other kernels (e.g., polynomial kernel, hybrid kernel [18]), which may yield potential improvements under certain conditions.

While the derivation is long, the online SVR algorithm at discrete time k can be summarized as follows - (1): obtain $\mathbf{y}_k$ from Eq.(31) and update $\mathbf{Y}_k$ in Eq.(37); (2): calculate $\hat{\Theta}_k$ and $\hat{\mathbf{b}}_k$ from Eq.(36); (3): obtain $\mathbf{u}_{k+1}$ based on Eq.(22) and calculate ψ_k in Eq.(40); (4): calculate γ_{k+1} for motion planning in Eq.(39); (5): iteratively update Π_k^{-1} through Eq.(41-48); and (6): return to Step (1) for discrete time $k+1$.

In the application, it should be noted that the model-based estimation of δ requires the inversion of matrix $\bar{\mathbf{M}}_2$, which requires the user to carefully design the exoskeleton controlled subsystem in Eq.(16b) to avoid numerical instability. Also, any significant perturbation $\mathbf{v}$ can undermine the motion planning performance due to poor estimation of the interaction load λ.

NUMERICAL SIMULATIONS

This section presents the control simulations of TAWE with the application of the proposed motion planning algorithm. The simulations are carried out in MATLAB [21]. The human-exoskeleton system of TAWE is modeled as a constrained closed-loop multibody system with two degrees of freedom (DOF) [5], which are q_{RUD} and q_{FE} on the wrist radial-ulnar deviation and flexion-extension directions, respectively.

The human input dynamics in real life is very complicated. In the simulations, we simplify the user input as the PID controller in Eq.(7) by default. The synthetic user motion intention, i.e., the tracking reference $\mathbf{r}_1$ for human control input $\mathbf{u}_1$ is a set of randomly generated quasi-periodic time series based on a frequency band of 0.2-0.4 Hz. Again, $\mathbf{r}_1$ is configured to be unknown to the TAWE controller. The simulation is performed on a sample rate of 1000 Hz, and the control input update rates for both $\mathbf{u}_1$ and $\mathbf{u}_2$ are 250 Hz. The default motion planning and controller parameters are selected as

$$\mathbf{C}_p = \mathbf{I}; \quad c_Q = 1\times 10^{-4}; \quad c_{\mathscr{K}} = 1; \quad m = 25 \tag{49a}$$

$$\mu = 25; \quad \mathbf{K}_1 = 4\mathbf{I}; \quad \mathbf{R}^{-1} = 0.0625\mathbf{I}; \quad \Gamma^{-1} = \mathbf{I} \tag{49b}$$

$$c_{u,1,\mathrm{P}} = 1; \quad c_{u,1,\mathrm{I}} = 0.0625; \quad c_{u,1,\mathrm{D}} = 0.25 \tag{49c}$$

Simulations without Disturbances

The first set of simulation trials are carried out in the zero-disturbance condition to observe the ideal performance of the motion planning algorithm. Under this condition, low-pass filters are not applied to the motion signals, which leads to $\mathbf{v} = \mathbf{0}$. Hence, Eq. (24) can provide an accurate estimation of δ.

We first observe the motion planning of $\mathbf{r}_2$ with the impedance term only. We also assume that the dynamical properties of the model (i.e., $\mathbf{M}$, $\mathbf{C}$, and $\mathbf{h}$) are known and implemented in $\mathbf{u}_1$ and $\mathbf{u}_2$, which are both designed as model-based PD controller (Eq.(11) without the adaptive term). The motion planning and trajectory tracking control results are shown in Figs. 3(a) and 3(b). While the impedance term can prevent the planned refer-

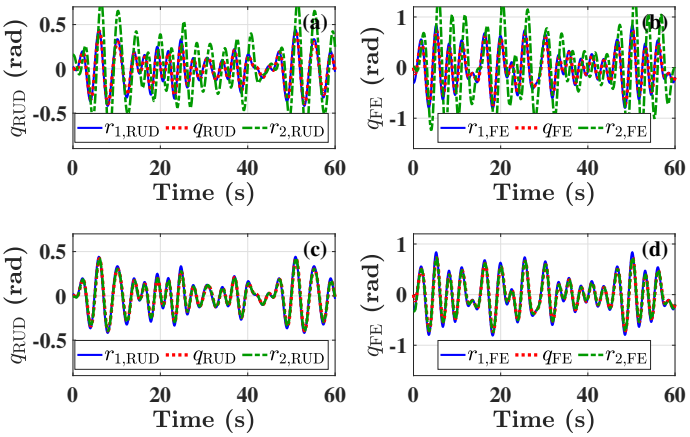

FIGURE 3: THE COMPARISON OF SYNTHETIC MOVEMENT INTENTION $\mathbf{r}_1$, SYSTEM STATE $\mathbf{q}$, AND EXOSKELETON REFERENCE $\mathbf{r}_2$ GENERATED BY MOTION PLANNING IN RUD (SUBFIGURES (a), (c)) AND FE (SUBFIGURES (b), (d)) DIRECTIONS, WHERE THE MOTION PLANNING IN SUBFIGURES (a) AND (b) INVOLVES THE IMPEDANCE TERM ONLY; THE MOTION PLANNING IN SUBFIGURES (c) AND (d) INVOLVES BOTH IMPEDANCE AND SVR TERMS.

ence $\mathbf{r}_2$ from drifting away from $\mathbf{q}$, $\mathbf{r}_2$ noticeably deviates from $\mathbf{r}_1$. The trajectories of $\mathbf{q}$ are attracted closer to $\mathbf{r}_1$, since $\mathbf{u}_1$ in this trial adopts a larger control gain ($\mathbf{R}^{-1} = 0.25\mathbf{I}$).

When the SVR model is activated, the exoskeleton reference $\mathbf{r}_2$ can closely approximate the synthetic movement intention $\mathbf{r}_1$, as shown in Figs. 3(c) and 3(d). We also notice that the trajectories of $\mathbf{q}$ and $\mathbf{r}_2$ converge with each other during steady states. It is important to show that $\mathbf{r}_2$ is not a random walk result, i.e., $\mathbf{r}_2$ being simply a delayed version of $\mathbf{q}$. Therefore, we closely compared $\mathbf{q}$ and $\mathbf{r}_2$ in the short-term as shown in Fig. 4. In Figs. 4(a) and 4(b), both $\mathbf{q}$ and $\mathbf{r}_2$ trajectories are declining along time, where the trajectory of $\mathbf{r}_2$ in Fig. 4(b) is ahead of $\mathbf{q}$. Similarly,

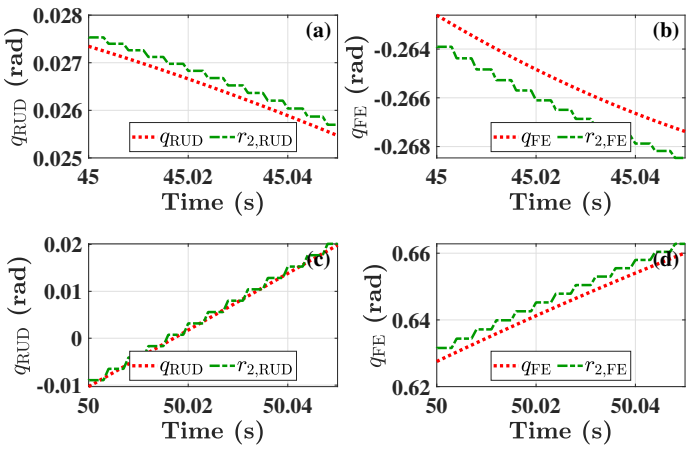

FIGURE 4: THE SHORT-TERM COMPARISON OF SYSTEM STATE $\mathbf{q}$ AND EXOSKELETON REFERENCE $\mathbf{r}_2$ GENERATED BY MOTION PLANNING IN RUD (SUBFIGURES (a), (c)) AND FE (SUBFIGURES (b), (d)) DIRECTIONS, WHERE SUBFIGURES (a) AND (b) SHOWS THE COMPARISON FOR A SHORT PERIOD OF TIME AFTER $t = 45$ s; SUBFIGURES (c) AND (d) SHOWS THE COMPARISON FOR A SHORT PERIOD OF TIME AFTER $t = 50$ s.

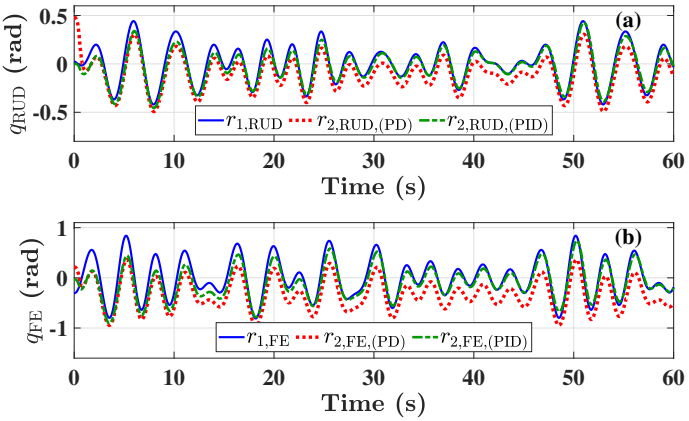

FIGURE 5: THE COMPARISON OF SYNTHETIC MOVEMENT INTENTION $\mathbf{r}_1$ AND EXOSKELETON REFERENCE $\mathbf{r}_2$ GENERATED BY MOTION PLANNING IN RUD (SUBFIGURE (a)) AND FE (SUBFIGURE (b)) DIRECTIONS, WHERE $\mathbf{r}_{2,\text{PD}}$ AND $\mathbf{r}_{2,\text{PID}}$ ARE GENERATED WHEN THE USER INPUT $\mathbf{u}_1$ IS RESPECTIVELY DESIGNED AS A PD CONTROLLER AND A PID CONTROLLER.

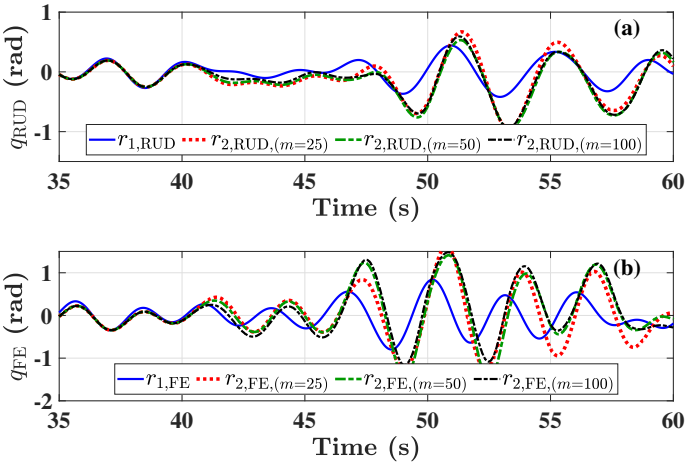

FIGURE 6: THE COMPARISON OF SYNTHETIC MOVEMENT INTENTION $\mathbf{R}_1$ AND EXOSKELETON REFERENCE $\mathbf{r}_2$ GENERATED BY MOTION PLANNING IN RUD (SUBFIGURE (a)) AND FE (SUBFIGURE (b)) DIRECTIONS, WHERE $\mathbf{r}_{2,\text{m=25}}$, $\mathbf{r}_{2,\text{m=50}}$, AND $\mathbf{r}_{2,\text{m=100}}$ ARE GENERATED BASED ON SVR DELAY PARAMETERS $m = 25$, $m = 50$, and $m = 100$, RESPECTIVELY. NOTE THAT THE UPDATE OF SVR MODEL PARAMETERS Θ AND $\mathbf{b}$ ARE STOPPED FOR ALL MOTION PLANNING AT $t = 40$ s.

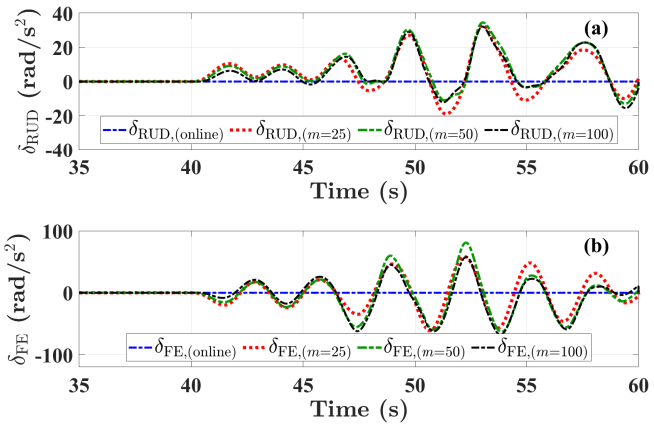

FIGURE 7: THE COMPARISON OF ESTIMATED INTERACTION LOADS δ IN RUD (SUBFIGURE (a)) AND FE (SUBFIGURE (b)) DIRECTIONS, CORRESPONDING TO THE DIFFERENT MOTION PLANNING CASES IN FIG. 6, WHERE $\mathbf{r}_{2,\mathrm{m=25}}$. HERE, $\mathbf{r}_{2,\mathrm{online}}$ IS GENERATED BY MOTION PLANNING ALGORITHM BASED ON THE DEFAULT PARAMETERS IN EQ.(49), WHERE THE SVR MODEL PARAMETER Θ AND $\mathbf{b}$ IS CONSTANTLY UPDATED. FOR THE OTHER CASES, THE UPDATES OF Θ AND $\mathbf{b}$ ARE STOPPED AT $t = 40$ s.

the trajectories of $\mathbf{r}_2$ are ahead of $\mathbf{q}$ during the climbing stage as shown in both Figs. 4(c) and 4(d). These results imply that $\mathbf{r}_2$ is not a random walk result. The lag of $\mathbf{r}_2$ in Fig. 4(a) is likely caused by the overshoot in the previous climbing stage.

When the dynamical properties are unknown, a PD controller $\mathbf{u}_1$ cannot compensate for the inertia and loads uncovered by $\mathbf{u}_2$, which results in steady-state tracking errors. In Fig. 5, we observe that such steady-state errors also result in $\mathbf{r}_2$ significantly deviated from $\mathbf{r}_1$ during steady states. On the other hand, with $\mathbf{u}_1$ designed as a PID controller, the steady-state deviation of $\mathbf{r}_2$ from $\mathbf{r}_1$ is eliminated. These results suggest that the motion planning algorithm is similar to a forecaster of $\mathbf{q}$ based on only the patterns of time-delayed data $\mathbf{q}$ and $\mathbf{r}_2$. The SVR model cannot infer steady-state errors between $\mathbf{q}$ and synthetic movement intention $\mathbf{r}_1$. Hence, $\mathbf{u}_1$ is designed as a PID controller with the default parameters in Eq.(49) in the following simulations.

Note that SVR model is not suitable for long-term regression, and the model parameter Θ and $\mathbf{b}$ used in Eq.(39) are required to be constantly updated. To demonstrate this, we compared the $\mathbf{r}_2$ trajectories generated under different delay parameters $m = 25$, $m = 50$, and $m = 100$, where for each case it is also configured that $\mu = m$. The results in Fig. 6 show similar performances from these three cases before $t = 40$ s, where all $\mathbf{r}_2$ trajectories accurately approximate $\mathbf{r}_1$. However, all $\mathbf{r}_2$ trajectories start to deviate from $\mathbf{r}_1$ after Θ and $\mathbf{b}$ stop updating at $t = 40$. The corresponding estimated interaction loads δ also significantly rise after $t = 40$ s, which implies that the obsolete Θ

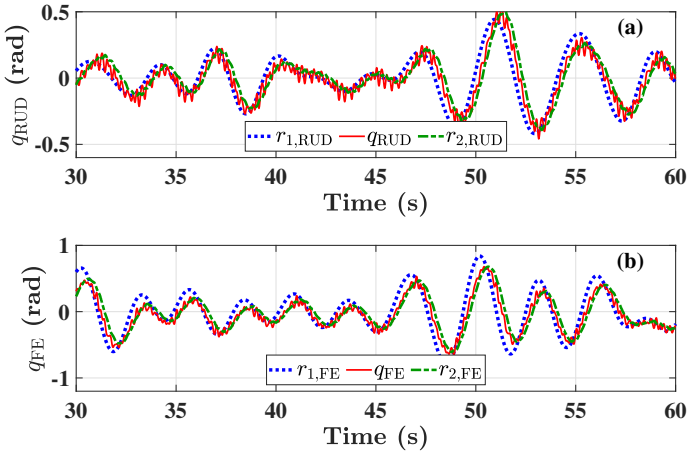

FIGURE 8: THE COMPARISON OF SYNTHETIC MOVEMENT INTENTION $\mathbf{r}_1$, SYSTEM STATE $\mathbf{q}$, AND EXOSKELETON REFERENCE $\mathbf{r}_2$ GENERATED BY MOTION PLANNING IN RUD (SUBFIGURE (a)) AND FE (SUBFIGURE (b)) dIRECTIONS, IN THE PRESENCE OF DISTURBANCES, NOISES, AND TREMORS.

and $\mathbf{b}$ can no longer provide accurate regression results.

Simulations with Disturbances

This subsection discusses the simulation results with the involvement of disturbances (above 10 Hz), sensor noises (above 10 Hz), and synthetic pathological tremors (3-6 Hz [22]), which are all randomly generated as quasiperiodic signals. In practice, the wrist kinematics of the user is not directly available and needs to be identified for the controller design [5, 13, 23]. Hence, we also

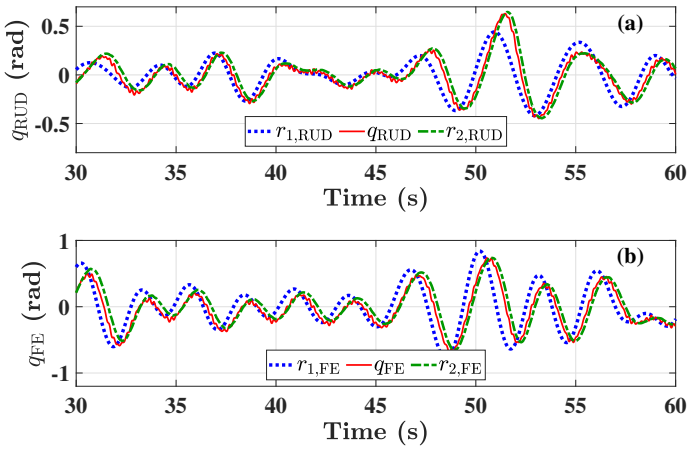

FIGURE 9: THE COMPARISON OF SYNTHETIC MOVEMENT INTENTION $\mathbf{r}_1$, SYSTEM STATE $\mathbf{q}$, AND EXOSKELETON REFERENCE $\mathbf{r}_2$ GENERATED BY MOTION PLANNING IN RUD (SUBFIGURE (a)) AND FE (SUBFIGURE (b)) DIRECTIONS, IN THE PRESENCE OF DISTURBANCES, NOISES, TREMORS, AND ACTIVE TREMOR SUPPRESSION THROUGH BMFLC.

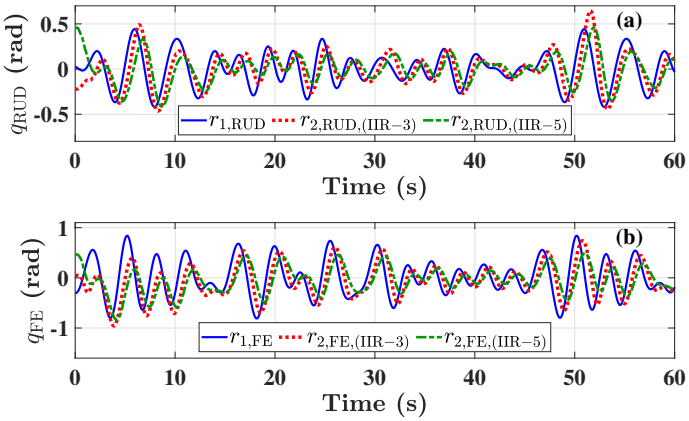

FIGURE 10: THE COMPARISON OF SYNTHETIC MOVEMENT INTENTION $\mathbf{r}_1$ AND EXOSKELETON REFERENCE $\mathbf{r}_2$ GENERATED BY MOTION PLANNING IN RUD (SUBFIGURE (a)) AND FE (SUBFIGURE (b)) DIRECTIONS, IN THE PRESENCE OF DISTURBANCES, NOISES, TREMORS, AND ACTIVE TREMOR SUPPRESSION THROUGH BMFLC. HERE, $\mathbf{r}_{2,\mathrm{IIR}-3}$ AND $\mathbf{r}_{2,\mathrm{IIR}-5}$ ARE GENERATED BY MOTION PLANNING WITH 3RD ORDER AND 5TH ORDER IIR FILTERS, RESPECTIVELY.

add to the simulation a real-time wrist kinematic identification (WKI) algorithm based on the Extended Kalman Filter [23, 24], which runs along with the controller and motion planning algorithm. The states $\mathbf{q}$ estimated through WKI are then low-pass filtered with a 3rd order Infinite Impulse Response (IIR) filter at 2 Hz. Finally, the delay parameters for SVR are selected as $m,\ \mu = 50$ for the following simulations.

The simulation results without tremor suppression is shown in Fig. 8. Without suppression, the synthetic tremors are also considered as disturbances, whose effects can be clearly observed from the small oscillations along the trajectories of $\mathbf{q}$. We also observe a significant delay of $\mathbf{q}$ and $\mathbf{r}_2$ from $\mathbf{r}_1$, which is mainly caused by the IIR filter. This delay affects the motion planning performance, and results in a noticeable deviation of $\mathbf{r}_2$ from $\mathbf{r}_1$. On the other hand, the trajectories of planned reference $\mathbf{r}_2$ based on the low-pass filtered states are much smoother compared to those of $\mathbf{q}$.

We then implemented the band-limited multi-frequency Fourier linear combiner (BMFLC) model for active tremor suppression [13,25], based on the assumption that tremor signals can be approximated by the linear combinations of harmonic waves of different frequencies from a certain bandwidth. The BMFLC compensator established on the matching bandwidth can be directly applied through the adaptive controller in Eq.(11), where the amplitudes of the harmonic waves are the unknown parameters constantly estimated by the update law in Eq.(11b). The simulations result with active tremor suppression are shown in Fig. 9, which shows that the oscillation amplitude in the trajectories of $\mathbf{q}$ are significantly reduced. The motion planning of $\mathbf{r}_2$, however, remains deviated from the synthetic movement intention $\mathbf{r}_1$ due to the delay introduced by the IIR filter.

To further observe the effect of delay caused by IIR filter, we compared the performances of motion planning under 3rd order and 5th order IIR filters. As shown in Fig. 10, the delay and inaccuracy of motion planning become more severe with the increase of filter order. Hence, it can be concluded that the major challenge is posed by delays introduced by filters, which can significantly affect the SVR regression and the motion planning performance.

In summary, we observe through simulations that the proposed motion planning algorithm can generate exoskeleton reference $\mathbf{r}_2$, which can closely approximate the synthetic movement intention $\mathbf{r}_1$ when the disturbance in the system is small. The algorithm can also be combined with the wrist kinematic identification algorithm and tremor suppression controller. However, the motion planning performance is limited in the presence of large disturbance and delays introduced by filters. Finally, the algorithm can run at a rate beyond 2000 Hz with SVR delay parameters $m,\ \mu = 50$ (on a AMD Ryzen 7 1800X CPU), making it efficient enough for real-time application.

CONCLUSION AND FUTURE WORK

This paper proposed a novel online modeled-based motion planning algorithm for a family of rehabilitation exoskeletons to improve transparency in user-guided operation. We first analyzed the dynamics of the human-exoskeleton control system. Based on the assumption that the human movement intention in the short-term can be embedded in the time-delay dimensions of motion signals, the model-based estimation was employed to obtain the interaction load between the dynamical subsystems respectively controlled by the human and exoskeleton. The objective of the motion planning algorithm was set to reduce the interaction load, which led to the establishment of a least-square optimization problem. A Support Vector Regression (SVR) model was then employed to solve the optimization problem by generating the exoskeleton tracking reference. We also designed the SVR model so that its properties can be calculated recursively for efficient real-time applications. The performance and characteristics of the motion planning algorithm were then observed and discussed through the control simulations of TAWE - a wearable wrist exoskeleton designed for pathological tremor alleviation. We observed that the planned tracking reference can approximate the synthetic human movement intention when the system disturbance is small. The algorithm can also be combined with the wrist kinematic identification algorithm and tremor suppression controller. However, the performance of the motion planning algorithm can be limited by system disturbances, and delays in signals introduced by filters.

For future works, we will investigate multi-step motion planning algorithms to overcome the effect of delays. We will also explore different optimization and regression model setups. Last

but most importantly, we will experiment the motion planning algorithm on human subjects through TAWE, and improve the performance and safety of the algorithm based on user feedback.

REFERENCES

[1] Maciejasz, P., Eschweiler, J., Gerlach-Hahn, K., Jansen-Troy, A., and Leonhardt, S., 2014. "A survey on robotic devices for upper limb rehabilitation". *Journal of neuroengineering and rehabilitation,* ***11***(1), p. 3.

[2] Fromme, N. P., Camenzind, M., Riener, R., and Rossi, R. M., 2019. "Need for mechanically and ergonomically enhanced tremor-suppression orthoses for the upper limb: a systematic review". *Journal of neuroengineering and rehabilitation,* ***16***(1), p. 93.

[3] Cao, F., Li, C., and Li, Y., 2015. "Robust sliding mode adaptive control for lower extremity exoskeleton". In 2015 Chinese Automation Congress (CAC), IEEE, pp. 400–405.

[4] Brahmi, B., Brahmi, A., Saad, M., Gauthier, G., and Habibur Rahman, M., 2019. "Robust adaptive tracking control of uncertain rehabilitation exoskeleton robot". *Journal of Dynamic Systems, Measurement, and Control,* ***141***(12).

[5] Wang, J., and Barry, O., 2021. "Inverse optimal robust adaptive controller for upper limb rehabilitation exoskeletons with inertia and load uncertainties". *IEEE Robotics and Automation Letters*.

[6] Zimmermann, Y., Kücüktabak, E. B., Farshidian, F., Riener, R., and Hutter, M., 2020. "Towards dynamic transparency: Robust interaction force tracking using multisensory control on an arm exoskeleton". In IEEE/RSJ International Conference on Intelligent Robots and Systems (IROS 2020)(virtual), pp. TuDT8–4.

[7] Just, F., Özen, Ö., Bösch, P., Bobrovsky, H., Klamroth-Marganska, V., Riener, R., and Rauter, G., 2018. "Exoskeleton transparency: feed-forward compensation vs. disturbance observer". *at-Automatisierungstechnik,* ***66***(12), pp. 1014–1026.

[8] Ajoudani, A., Zanchettin, A. M., Ivaldi, S., Albu-Schäffer, A., Kosuge, K., and Khatib, O., 2018. "Progress and prospects of the human–robot collaboration". *Autonomous Robots,* ***42***(5), pp. 957–975.

[9] Li, Z., Su, C.-Y., Wang, L., Chen, Z., and Chai, T., 2015. "Nonlinear disturbance observer-based control design for a robotic exoskeleton incorporating fuzzy approximation". *IEEE Transactions on Industrial Electronics,* ***62***(9), pp. 5763–5775.

[10] Jarrassé, N., Paik, J., Pasqui, V., and Morel, G., 2008. "How can human motion prediction increase transparency?". In 2008 IEEE International Conference on Robotics and Automation, IEEE, pp. 2134–2139.

[11] Chen, X., Zeng, Y., and Yin, Y., 2016. "Improving the transparency of an exoskeleton knee joint based on the understanding of motor intent using energy kernel method of emg". *IEEE Transactions on Neural Systems and Rehabilitation Engineering,* ***25***(6), pp. 577–588.

[12] Shen, Y., Sun, J., Ma, J., and Rosen, J., 2019. "Admittance control scheme comparison of exo-ul8: A dual-arm exoskeleton robotic system". In 2019 IEEE 16th International Conference on Rehabilitation Robotics (ICORR), IEEE, pp. 611–617.

[13] Wang, J., and Barry, O., 2020. "Multibody analysis and control of a full-wrist exoskeleton for tremor alleviation". *Journal of Biomechanical Engineering*.

[14] Takens, F., 1981. "Detecting strange attractors in turbulence". In *Dynamical systems and turbulence, Warwick 1980*. Springer, pp. 366–381.

[15] Sartori, M., Lloyd, D. G., and Farina, D., 2016. "Neural data-driven musculoskeletal modeling for personalized neurorehabilitation technologies (vol 63, pg 879, 2016)". *IEEE Transactions on Biomedical Engineering,* ***63***(6), pp. 1341–1341.

[16] Smola, A. J., and Schölkopf, B., 2004. "A tutorial on support vector regression". *Statistics and computing,* ***14***(3), pp. 199–222.

[17] Tatinati, S., Veluvolu, K. C., and Ang, W. T., 2014. "Multistep prediction of physiological tremor based on machine learning for robotics assisted microsurgery". *IEEE transactions on cybernetics,* ***45***(2), pp. 328–339.

[18] Yang, C., Luo, J., Pan, Y., Liu, Z., and Su, C.-Y., 2017. "Personalized variable gain control with tremor attenuation for robot teleoperation". *IEEE Transactions on Systems, Man, and Cybernetics: Systems,* ***48***(10), pp. 1759–1770.

[19] Chang, Y.-W., Hsieh, C.-J., Chang, K.-W., Ringgaard, M., and Lin, C.-J., 2010. "Training and testing low-degree polynomial data mappings via linear svm.". *Journal of Machine Learning Research,* ***11***(4).

[20] Zhang, F., 2006. *The Schur complement and its applications*, Vol. 4. Springer Science & Business Media.

[21] Wang, J., Kamidi, V. R., and Ben-Tzvi, P., 2018. "A multibody toolbox for hybrid dynamic system modeling based on nonholonomic symbolic formalism". In ASME 2018 Dynamic Systems and Control Conference, American Society of Mechanical Engineers, pp. V003T29A003–V003T29A003.

[22] Kalia, L. V., and Lang, A. E., 2015. "Parkinson's disease". *The Lancet,* ***386***(9996), pp. 896 – 912.

[23] Wang, J., and Barry, O., 2021. "Real-time identification of wrist kinematics via sparsity-promoting extended kalman filter based on ellipsoidal joint formulation". *(Submitted to) IEEE Transactions on Biomedical Engineering*.

[24] Haykin, S. S., 2005. *Adaptive filter theory*. Pearson Education India.

[25] Veluvolu, K. C., and Ang, W. T., 2011. "Estimation of physiological tremor from accelerometers for real-time applications". *Sensors,* ***11***(3), pp. 3020–3036.